# From CO or $CO_2$?
# Space-resolved insights into high-pressure $CO_2$ hydrogenation to methanol over $Cu/ZnO/Al_2O_3$

Gaikwad, Rohit; Reymond, Helena; Phongprueksathat, Nat; Rudolf Von Rohr, Philipp; Urakawa, Atsushi

**DOI**
10.1039/d0cy00050g

**Publication date**
2020

**Document Version**
Final published version

**Published in**
Catalysis Science and Technology

Catalysis Science & Technology

ROYAL SOCIETY OF CHEMISTRY

COMMUNICATION

View Article Online
View Journal | View Issue



Cite this: *Catal. Sci. Technol.*, 2020, **10**, 2763

Received 14th January 2020,
Accepted 5th March 2020

DOI: 10.1039/d0cy00050g

rsc.li/catalysis

# From CO or $CO_2$?: space-resolved insights into high-pressure $CO_2$ hydrogenation to methanol over $Cu/ZnO/Al_2O_3$†

Rohit Gaikwad,‡[a] Helena Reymond,‡[b] Nat Phongprueksathat,‡[ac] Philipp Rudolf von Rohr[b] and Atsushi Urakawa *[acd]

**The reaction pathway of high-pressure $CO_2$ hydrogenation over a $Cu/ZnO/Al_2O_3$ catalyst is investigated through the gradients of reactants/products concentration and catalyst temperature within the catalytic reactor. This study reveals that methanol is formed through direct $CO_2$ hydrogenation at low temperature, while above 260 °C methanol formation is mediated *via* CO which is formed by reverse water–gas shift reaction.**

The increasing atmospheric $CO_2$ concentration demands urgent actions to reduce $CO_2$ emission by converting $CO_2$ into useful chemicals and fuels. Among various chemicals derived from $CO_2$, methanol has considerable potential as a liquid fuel, hydrogen carrier, and $C_1$ feedstock.[1,2] Methanol can now be synthesized on commercially relevant scales *via* $CO_2$ hydrogenation over $Cu/ZnO/Al_2O_3$-based catalysts at 200–300 °C and 10–100 bar,[3,4] which is by far the most mature technology for efficient $CO_2$ conversion.[1] From a mechanistic point of view, methanol synthesis from $CO_2$ over $Cu/ZnO/Al_2O_3$ catalysts may occur through direct $CO_2$ hydrogenation (eqn (1)) or through reverse water–gas shift (RWGS) (eqn (2)) followed by CO hydrogenation (eqn (3)).[2]

$$CO_2 + 3H_2 \rightleftharpoons CH_3OH + H_2O \quad \Delta H_{298K,5MPa} = -40.9 \text{ kJ mol}^{-1} \quad (1)$$

$$CO_2 + H_2 \rightleftharpoons CO + H_2O \quad \Delta H_{298K,5MPa} = +49.8 \text{ kJ mol}^{-1} \quad (2)$$

$$CO + 2H_2 \rightleftharpoons CH_3OH \quad \Delta H_{298K,5Mpa} = -90.7 \text{ kJ mol}^{-1} \quad (3)$$

Since methanol synthesis from $CO_2$ accompanies CO formation, the early studies concluded that CO hydrogenation is the main reaction pathway over Cu/ZnO catalysts.[5–7] However, the $C^{18}O_2$ isotopic labeling indicated that methanol can be produced from both CO and $CO_2$, by which $CO_2$ hydrogenation is the primary pathway at 220 °C.[8] The $^{14}CO$ and $^{14}CO_2$ isotopic labeling also supported that $CO_2$ is the primary source of methanol instead of CO at 250 °C.[9] The intrinsic $CO_2$ hydrogenation rate is ~20 times faster than CO hydrogenation, especially at low conversion,[10] although the $CO_2$ hydrogenation is suppressed at high conversion due to water formation.[11] In contrast, DFT calculations showed the rate of the RWGS to form CO becomes ~100 times higher than $CO_2$ hydrogenation to methanol at a higher temperature (300 °C), in agreement with experiment.[12] However, such CO rather accumulates as a product since CO hydrogenation is slower than $CO_2$ hydrogenation. Another set of DFT calculations fitted to published experimental rate data under realistic conditions suggested that $CO_2$ hydrogenation is responsible for ~2/3 of methanol production.[13] It was later confirmed by isotope tracing experiments in $^{13}CO/^{12}CO_2/H_2$ that $CO_2$ is the dominant carbon source in methanol product at 240 °C. However, the source of carbon gradually shifts from $CO_2$ to CO as the temperature is lowered (toward 160 °C).[14] It was proposed that CO hydrogenation could also be inhibited by the formation of formate intermediates at higher $CO_2$ concentrations (230 °C).[15,16] The isotopic labeling using H/D substitution suggested that methanol formation from $CO_2$ does not occur *via* consecutive RWGS and CO hydrogenation (at 250 °C),[17] and rather RWGS and $CO_2$ hydrogenation occur independently (220–260 °C).[17,18] Although some debates exist, methanol formation from $CO_2$ as the carbon source is currently the most widely accepted mechanism for Cu/ZnO-based catalysts, supported by both experimental findings and theoretical calculations mentioned above.

Thermodynamically, both CO and $CO_2$ hydrogenation reactions produce methanol, but the predominant reactions depend on the operating conditions.[19] The favorable conditions

[a] *Institute of Chemical Research of Catalonia (ICIQ), Av. Països Catalans 16, 43007 Tarragona, Spain*
[b] *Department of Mechanical Engineering, Institute of Process Engineering, ETH Zurich, Sonneggstrasse 3, 8092 Zürich, Switzerland*
[c] *Catalysis Engineering, Department of Chemical Engineering, Delft University of Technology, Van der Maasweg 9, 2629 HZ Delft, Netherlands. E-mail: A.Urakawa@tudelft.nl*
[d] *Japan Science and Technology Agency (JST), Gobancho, Chiyodaku, 102-0076 Tokyo, Japan*

† Electronic supplementary information (ESI) available. See DOI: 10.1039/d0cy00050g

‡ The three first authors contributed equally to this work.

for $CO_2$ hydrogenation to methanol are high pressure and low temperature according to Le Châtelier's principle, as obvious from eqn (1),[2] and the advantages of high-pressure reaction conditions above 200 bar in terms of $CO_2$ conversion (>90%), methanol selectivity (>95%) and methanol yield have been recently demonstrated.[20,21] In practice, however, there is an optimum reaction temperature where reaction kinetics are favorable, and simultaneously, endothermic RWGS does not rule the product selectivity. For example, in the previous studies (200 and 360 bar), the CO selectivity is surprisingly high at 170–200 °C, while it starts to decrease to the minimum as the temperature increases to 260 °C, indicating the CO hydrogenation towards the formation of methanol.[21] Similarly, CO selectivity increases at high space velocities, implying that CO-mediated path may be active under high-pressure conditions, which is indeed in accordance with early study at high pressure (415 bar).[5] Most mechanistic studies aiming at elucidation of the reaction pathway are performed at low to moderate pressure (<30 bar) and there are no convincing mechanistic clues reported to date for high-pressure methanol synthesis above such pressure.

This study aims at clarifying dominating reaction pathways and the source of carbon, CO or $CO_2$, resulting in methanol from the concentration profiles of the reactants/products as well as that of the catalyst temperature along the axial direction of the reactor packed with a commercial Cu/ZnO/$Al_2O_3$ catalyst at 200 and 360 bar (reactant pressure of 184 and 331 bar).[20,21] Changing space velocity by varying the reactant flow rate and/or catalyst amount is one way to gain the information;[22] however, this approach may influence mass transfer characteristics and also temperature gradient (higher mass flow rate can results in more prominent temperature gradient due to endo-/exo-thermicity of the reactions). In this study, we developed a method to study quantitatively the concentration of reactant/product fluids based on gas chromatography (GC) and Raman spectroscopy looking at different locations of the catalyst bed. Furthermore, infrared (IR) thermography was used to monitor the catalyst temperature under *operando* high-pressure reaction conditions to gain support on the reaction mechanisms through exo- and endothermicity.

The high-pressure reactor setup and used materials are explained in detail in ESI.† Briefly, the commercial Cu/ZnO/$Al_2O_3$ catalyst[20] was packed in a stainless steel (SS) or sapphire capillary reactor where three split catalyst beds were separated by empty spaces (*P*1–*P*4) for gas sampling and quantification. In the case of the SS reactor (Fig. 1A), the gas sampling for GC analysis was performed by needle valves connected to the void sections. The amount of the sampled gas was sufficiently small (confirmed by GC) so that it did not affect the overall catalytic activity. For Raman spectroscopic determination of fluid concentration, a Raman laser (532 nm) was focused onto the void sections filled with quartz wool in the sapphire reactor (Fig. 1B, S1 and S2,† holding reactant pressure up to 200 bar, 350 °C). The major advantage of the GC analysis is the accuracy in the quantification and that of the Raman analysis is the non-perturbing nature of the sampling on the flow behavior.

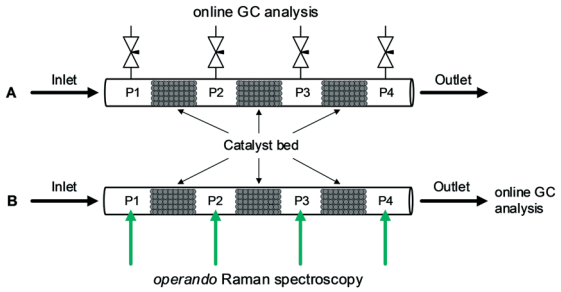


**Fig. 1** Schematic of catalyst beds configuration for (A) a stainless-steel reactor with gas sampling valves at *P*1–*P*4, and (B) a sapphire reactor with Raman spectroscopic gas analysis at *P*1–*P*4 and gas chromatographic analysis at the outlet.

First, concentration profiling at *P*1–*P*4 was performed during $CO_2$ hydrogenation at the stoichiometric ratio ($H_2/CO_2$ = 3) in the SS reactor at three temperatures (180, 260 and 340 °C) and two pressure conditions (184 and 331 bar). $CO_2$ conversion and carbon-based mole fractions *F* (both in %), which are defined as $CO_2$ conversion scaled by respective product selectivity (that is in 0–1 scale, leading to $F_{CH_3OH} + F_{CO} = X_{CO_2}$). These quantities were used to understand in a facile fashion how much $CO_2$ is converted and into which product.

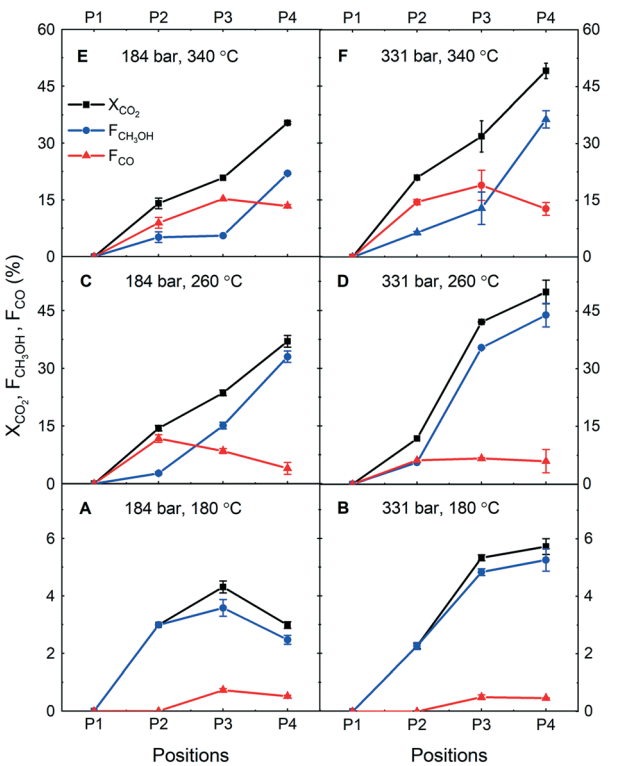


**Fig. 2** $CO_2$ conversion ($X_{CO_2}$), the mole fraction of methanol ($F_{CH_3OH}$) and CO ($F_{CO}$) at different axial positions (*P*1–*P*4) during $CO_2$ hydrogenation to methanol over the commercial Cu/ZnO/$Al_2O_3$ catalyst. $H_2/CO_2$ = 3, *T* = 180, 260, and 340 °C, *P* = 184 and 331 bar, and GHSV = 10 000 $h^{-1}$.

Fig. 2A and B show the catalytic performance in terms of $X_{CO_2}$, $F_{CH_3OH}$ and $F_{CO}$ at 180 °C at 184 bar and 331 bar, respectively. At this low reaction temperature, we observe low $CO_2$ conversion but high methanol selectivity, thus a high fraction of methanol. What is prominent are the *X* and *F* profiles and their differences. At this low conversion, virtually the partial pressure of the reactants ($CO_2$ and $H_2$) is unaltered throughout the catalyst bed and generally one expects little change in the reaction rate and product selectivity due to full kinetic control at different positions of the catalyst bed. However, this is not the case and lower $CO_2$ conversion is more prominent at the lower investigated pressure (184 bar, Fig. 2A) where $CO_2$ conversion does not linearly increase between *P*2–*P*3, and even drops between *P*3–*P*4. When the rate of $CO_2$ conversion is decreased, the fraction of methanol also decreases. Assuming that the intrinsic reaction selectivity at this temperature is almost 100% towards methanol (judging from the values at *P*2), the only explanation for the $CO_2$ conversion drop is methanol decomposition ($CH_3OH \rightarrow CO + 2H_2$),[23] especially between *P*2–*P*3. However, since the water partial pressure is expected to rise along with along the catalyst bed and the $CO_2$ conversion between *P*3–*P*4, steam reforming ($CH_3OH + H_2O \rightarrow CO_2 + 3H_2$) is supposed to take place. Although the reports on gas-phase methanol decomposition and steam reforming at such high pressure are expectedly limited, there is evidence suggesting that such reactions occur even at 250–450 bar under supercritical water,[24] and its kinetics can be enhanced as the number of collisions increases with pressure. Moreover, the slight decrease in CO fraction also indicates the forward water gas shift reaction. This explanation is also in accordance with high CO selectivity at low temperatures, as found in the previous work.[21] Based on the profiles of $CO_2$ conversion and product fractions, at 331 bar (Fig. 2B) this methanol decomposition and steam reforming to CO and $CO_2$ (generalized as "methanol decompositions") also takes place but to a significantly lesser extent. This is likely due to the pressure effects affecting to shift the equilibrium towards the product (methanol) side, showing one of the unique advantages of high-pressure reaction conditions.[20,21]

The same experiment was performed at two higher temperatures (260 and 340 °C) and the results obtained at 260 °C are summarized in Fig. 2C and D. First, the $CO_2$ conversion values are about one order of magnitude higher than those at 180 °C. Also, at both examined pressures, relatively high CO selectivity was observed. At 184 bar (Fig. 2C), CO was the major product, but then the fraction of CO decreased towards the outlet position. This is indicative of CO conversion to methanol, although there is a possibility of water–gas shift reaction forming $CO_2$ and $H_2$ from CO and $H_2O$ (reverse reaction of eqn (2)). However, the methanol fraction drastically increases as CO fraction dropped towards the outlet direction. This indicates the former reaction (*i.e.* CO hydrogenation to methanol, eqn (3)) is likely the major active path under the studied reaction condition. At 331 bar (Fig. 2D) CO fraction remained relatively constant, whereas the methanol fraction increased drastically along with $CO_2$ conversion between *P*2 and *P*3. At 184 bar (Fig. 2C) $CO_2$ conversion linearly increased and did not drop as observed at 180 °C. These results indicate three important insights into high-pressure $CO_2$ hydrogenation at 260 °C: (i) methanol formation is faster than its decompositions, (ii) $CO_2$ is constantly converted to methanol or CO as the intermediate at 184 bar and (iii) there is another factor promoting/enhancing $CO_2$ conversion at 331 bar. Regarding the point (ii), at 184 bar at *P*2, very high CO selectivity was observed and its continuous decrease and drastic increase in methanol production towards the reactor outlet implies that $CO_2$ is converted to CO at an almost constant rate and then CO is further converted to methanol. In this case, the latter reaction rate would mainly determine the final fraction of methanol and CO in the reactor. The point (iii) indicates the important effects of reaction pressure. According to Fig. S4 (ESI†), at 260 °C, we expect phase condensation at 331 bar but not at 184 bar. This may explain the sudden surge in $CO_2$ conversion between *P*2–*P*3; the $CO_2$ conversion was sufficiently high to reach the dew point of the condensable products (methanol and water) at this position in the reactor, positively impacting on the reaction rate or shifting the equilibrium towards methanol.

The presence of water in the fluid phase can promote Cu crystallite growth[25] and induce transformation of ZnO into $ZnCO_3$, as shown in the XRD patterns of spent catalysts (Fig. S3 and Table S1, ESI†). However, it is still difficult to establish the relationship between mechanism and catalyst structure from the existing results, especially using the bulk sensitive techniques.

Furthermore, the results obtained at the highest examined temperature (340 °C) are presented in Fig. 2E and F. Similar to the case of 260 °C, a large amount of CO was observed with a decrease in its fraction with respect to methanol towards the reactor outlet. On the other hand, $CO_2$ conversion increased almost linearly. These two observations indicate that RWGS is the first main step of $CO_2$ hydrogenation and produced CO reacts further with $H_2$ to produce methanol. It is also interesting to note the boosted methanol formation between *P*3–*P*4. A similar observation at 260 °C was interpreted to be caused by phase condensation. At this temperature, however, we do not expect such phase condensation to occur (Fig. S4, ESI†). One possibility may be a dense phase formation, like surface wetting, in the pore of the catalyst which is virtually identical to phase condensation. Besides, it is worth highlighting the maximum CO fraction observed in the reactor at 260 and 340 °C. According to the thermodynamic calculation (Fig. S5, ESI†), the equilibrium $CO_2$ conversions for RWGS at $H_2/CO_2 = 3$ are *ca.* 14% and 21% at 260 and 340 °C, respectively. A careful look in Fig. 2E and F shows that the CO fraction is close to the equilibrium $CO_2$ conversion in the middle of the reactor (since the fraction is the percentage of $CO_2$ converted to methanol; therefore, these numbers can be directly compared). Still, the CO fraction decreases accompanying the increase in methanol fraction close to the outlet of the reactor, implying that the

methanol synthesis rate is accelerated at the position. It is speculated that the dense phase formation over the catalyst accelerates CO hydrogenation to methanol. In addition, methanol decompositions may take place, but it is not possible to gain information about this point from the data obtained. Nevertheless, it is certain that the consumption rate of CO and $CO_2$ to form methanol is much greater than the methanol decompositions rate under these high-pressure conditions.

Based on the above studies, we conclude that the pressure effects on the reaction paths are relatively minor compared to the temperature effects, although increasing pressure is indeed advantageous for methanol synthesis because of favorable kinetics (more collisions), phase separation, and chemical equilibrium.[26] Interestingly, at 260 °C where we find optimum catalytic performance and liquid-phase condensation seems indeed to boost the reactivity of $CO_2$ to methanol by a concerted kinetic and thermodynamic interplay.

Furthermore, similar concentration profiling experiments were performed using Raman spectroscopy instead of GC. The major advantage of this spectroscopic approach is that the reaction and flow-patterns are not disturbed in contrast to the case of GC analyses. Fig. S6 (ESI†) shows a typical Raman spectrum of the reaction stream obtained at 260 °C at the outlet (*P*4). The rotational transitions of $H_2$ (355, 587, 812, 1033, 1246, 1447 $cm^{-1}$), as well as the Fermi dyad of $CO_2$ and satellite bands (1265, 1286, 1387, 1408 $cm^{-1}$), were clearly identified. Because of the small Raman scattering cross-section of CO, its characteristic feature at 2140 $cm^{-1}$ was not sufficiently strong for quantitative analysis and only its formation could be confirmed at high CO concentration. The features at 2840 and 2945 $cm^{-1}$ are attributed to methanol, showing a too weak signal for quantitative analysis. For these reasons, the intense bands of $H_2$ and $CO_2$ at 587 and 1387 $cm^{-1}$, respectively, were considered here to gain mechanistic insights.

Fig. 3 shows the evolution of the $H_2/CO_2$ ratio determined from the band areas at different void positions (Fig. 1) at 180 °C and 260 °C at 184 bar. The initial area ratio at *P*1 was scaled to 2.5 to represent the molar ratio of unreacted feed confirmed by GC measurements. The reaction at 180 °C showed a slight decrease in the ratio moving from *P*1 to *P*2, before increasing towards *P*3, and no major change was observed moving from *P*3 to *P*4.

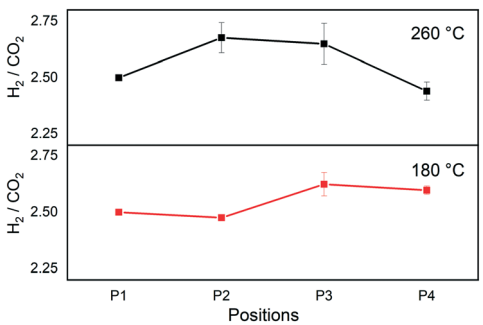


**Fig. 3** $H_2/CO_2$ ratio at different positions during $CO_2$ hydrogenation to methanol over the commercial $Cu/ZnO/Al_2O_3$ catalyst. $H_2/CO_2$ = 2.5, *T* = 180 and 260 °C, *P* = 184 bar, and GHSV = 80 000 $h^{-1}$.

In the case of direct methanol synthesis from $CO_2$ (eqn (1)), 3 moles of $H_2$ would be consumed per mole of $CO_2$ for the production of methanol, rendering $H_2$ the limiting reactant in our experimental condition (feed $H_2/CO_2$ = 2.5). On the other hand, if $CO_2$ is consumed to form CO *via* RWGS (eqn (2)), $CO_2$ would become a limiting reactant. Therefore, a decrease in the $H_2/CO_2$ ratio would signify an excessive $H_2$ consumption as in the former case of direct methanol synthesis, whereas an increase in the ratio would be a sign of a gradual $CO_2$ shortage by RWGS. In case methanol is a secondary product obtained from the subsequent hydrogenation of CO, as a net, the ratio is expected to decrease as an equivalent amount of $H_2$ is required whichever the $CO_x$ ($x$ = 1 or 2) is the carbon source in the methanol. The initial slight decrease in the ratio at *P*1–*P*2 at 180 °C implies direct methanol synthesis reaction. Then at *P*2–*P*3, the ratio increases, which is indicative of RWGS. However, as discussed above, this is most likely due to the decompositions of methanol since such drastic selectivity change is unlikely at the low $CO_2$ conversion level. The increase in the ratio is therefore attributed to methanol decompositions, which is fully consistent with the observation and the previous results at 180 °C (Fig. 2). In this Raman study, however, the ratio did not increase further as expected from the results in Fig. 2. This may be due to the higher space velocity of this Raman study compared to the study by GC and consequent less pronounced change in the ratio from less prominent methanol decompositions.

At 260 °C there was a clear initial increase of the ratio and then decrease towards the outlet (Fig. 3). The increasing ratio indicates the increase in the amount of CO by RWGS in the reactor and then subsequent decrease indicates the increase in the amount of methanol, no matter which reaction paths (eqn (1) *vs.* eqn (3)) are active. This profile is in full accordance with the results presented in Fig. 2 obtained in a comparable reaction condition where initially CO was produced and then CO was hydrogenated to methanol.

The sharp drop in the ratio at 260 °C coincided with the observation of condensation as liquid droplets at the rear end of the packed bed at *P*4 (Fig. S8, ESI†). As discussed above, the condensation is attributed to enhanced methanol synthesis *via* CO or $CO_2$, by *in situ* separation of the less volatile components, namely water and methanol. Indeed, upon focusing the Raman laser spot on the condensed phase, more intense methanol peak was observed, and the $H_2/CO_2$ ratio dropped to further lower values, suggesting the higher miscibility of $CO_2$ than $H_2$ in the condensed phase. According to the thermodynamic expectations at $CO_2:H_2$ = 1 : 3 (Fig. S4, ESI†), liquid phase condensation is not expected at 184 bar, 260 °C.

Lastly, IR thermography was used to measure the temperature of the catalyst bed under the reaction in order to validate the sequential nature of the methanol formation (RWGS and CO hydrogenation to methanol) from the endo-/exo-

 

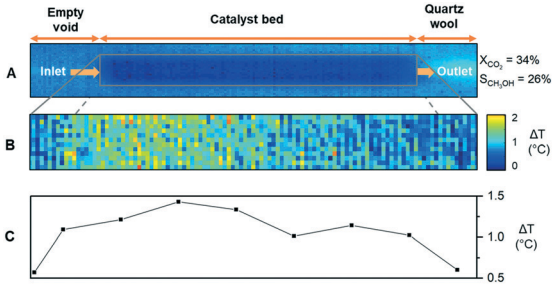


**Fig. 4** (A) IR thermogram of catalyst bed at room temperature, (B) subtracted IR thermogram at reaction temperature, and (C) temperature deviation ($\Delta T$) profile along the catalyst bed during $CO_2$ hydrogenation to methanol over the commercial $Cu/ZnO/Al_2O_3$ catalyst. $H_2/CO_2$ = 3, $T$ = 340 °C, $P$ = 184 bar, and GHSV = 80 000 $h^{-1}$.

thermicity of the reactions (eqn (1)–(3)). The reaction was performed at the stoichiometric ratio at 184 bar in a sapphire reactor similar to the Raman study without separating the catalyst bed, as shown in Fig. 4A. At 180 °C, the IR signal, as well as $CO_2$ conversion, were too low to detect changes in the temperature of the catalyst bed. Thus, the experiments were performed at 260 and 340 °C. To detect subtle differences in the temperature of the catalyst bed, the thermogram showing a temperature distribution is obtained by the subtraction of thermograms during reaction and calibration, as shown in Fig. S9 (ESI†).

The differential IR thermogram (Fig. 4B) displays an exothermic region of the catalyst bed during the reaction. The differential temperature profiles (Fig. 4C) are calculated from the radial temperature average along the catalyst bed. Evidently, the temperature profile at 340 °C is spatially varying. A relatively colder region located close to the front of the catalyst bed at 340 °C and subsequent temperature increase (then decrease) along the flow direction indicate endothermicity of RWGS near the fluid inlet and then methanol is formed. Such a temperature variation along the catalyst bed is barely observable at 260 °C (Fig. S10†), indicating that RWGS and CO hydrogenation likely occur in close proximity and cause overlapping of the two regions. The results at two different temperatures are in line with the methanol and CO selectivity profiles and the reaction mechanisms suggested above.

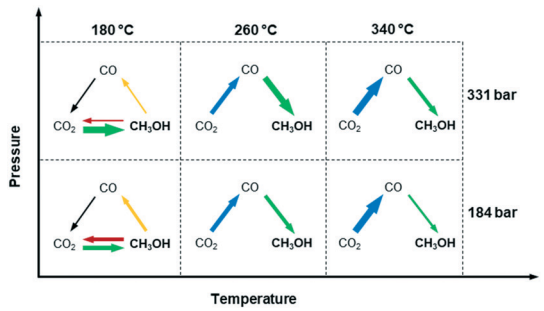


**Fig. 5** Major reaction pathways in high-pressure $CO_2$ hydrogenation over $Cu/ZnO/Al_2O_3$ catalyst at 180 °C, 260 °C and 340 °C at 184 and 331 bar. The width of the arrow shows the amount of one species transformation to others.

In conclusion, the effects of temperature and pressure on reaction pathways were clarified by the space-resolved methodologies under *operando* conditions. Temperature has a significant influence on the dominant reaction pathways of methanol synthesis, as summarized in Fig. 5. It is confirmed that methanol is produced *via* direct $CO_2$ hydrogenation at 180 °C, and *via* RWGS and CO hydrogenation at 260–340 °C. This could be explained by the limited RWGS activity at 180 °C, and more dominant RWGS activity as temperature increases. Moreover, there is a sign that methanol could possibly decompose or be steam reformed after formation, which is effectively suppressed by increasing pressure. Although pressure seems to have no influence on the reaction pathways, it greatly enhances methanol selectivity by inducing *in situ* condensation. This work demonstrates how spatially resolved *operando* study can be performed at high-pressure conditions to gain insights into the reaction mechanisms that have practical implications of potential advantages of multicomponent catalysts (*i.e.* selective in CO or $CO_2$ to methanol) in a reactor.

## Conflicts of interest

There are no conflicts to declare.

## Acknowledgements

Financial support from the Swiss National Science Foundation (Sinergia grant no. CRSII2-154448 and CRSII5-183495) are greatly acknowledged. R. G., N. P. and A. U. acknowledge Generalitat de Catalunya for financial support through the CERCA Programme and MINECO, Spain for financial support (CTQ2016-75499-R (FEDER-UE), SEV-2013-0319). A. U. thanks JST PRESTO (grant no. JPMJPR16S3).

## References

1 A. Goeppert, M. Czaun, J.-P. Jones, G. K. Surya Prakash and G. A. Olah, *Chem. Soc. Rev.*, 2014, **43**, 7995–8048.
2 A. Álvarez, A. Bansode, A. Urakawa, A. V. Bavykina, T. A. Wezendonk, M. Makkee, J. Gascon and F. Kapteijn, *Chem. Rev.*, 2017, **117**, 9804–9838.
3 G. A. Olah, *Angew. Chem., Int. Ed.*, 2013, **52**, 104–107.
4 G. A. Olah, A. Goeppert and G. K. S. Prakash, *Beyond Oil and Gas: The Methanol Economy*, Wiley, 2009, vol. 44.
5 V. N. Ipatieff and G. S. Monroe, *J. Am. Chem. Soc.*, 1945, **67**, 2168–2171.
6 K. Klier, *Adv. Catal.*, 1982, **31**, 243–313.
7 K. Klier, V. Chatikavanij, R. G. Herman and G. W. Simmons, *J. Catal.*, 1982, **74**, 343–360.
8 G. Liu, D. Willcox, M. Garland and H. H. Kung, *J. Catal.*, 1985, **96**, 251–260.
9 G. C. Chinchen, P. J. Denny, D. G. Parker, M. S. Spencer and D. A. Whan, *Appl. Catal.*, 1987, **30**, 333–338.
10 M. Sahibzada, I. S. Metcalfe and D. Chadwick, *J. Catal.*, 1998, **174**, 111–118.
11 C. V. Ovesen, B. S. Clausen, J. Schiøtz, P. Stoltze, H. Topsøe and J. K. Nørskov, *J. Catal.*, 1997, **168**, 133–142.

12 Y. Yang, J. Evans, J. A. Rodriguez, M. G. White and P. Liu, *Phys. Chem. Chem. Phys.*, 2010, **12**, 9909.
13 L. C. Grabow and M. Mavrikakis, *ACS Catal.*, 2011, **1**, 365–384.
14 Y. Yang, C. A. Mims, D. H. Mei, C. H. F. Peden and C. T. Campbell, *J. Catal.*, 2013, **298**, 10–17.
15 F. Studt, M. Behrens, E. L. Kunkes, N. Thomas, S. Zander, A. Tarasov, J. Schumann, E. Frei, J. B. Varley, F. Abild-Pedersen, J. K. Nørskov and R. Schlögl, *ChemCatChem*, 2015, **7**, 1105–1111.
16 W. J. Van Rensburg, M. A. Petersen, M. S. Datt, J. A. Van Den Berg and P. Van Helden, *Catal. Lett.*, 2015, **145**, 559–568.
17 E. L. Kunkes, F. Studt, F. Abild-Pedersen, R. Schlögl and M. Behrens, *J. Catal.*, 2015, **328**, 43–48.
18 A. Karelovic, G. Galdames, J. C. Medina, C. Yévenes, Y. Barra and R. Jiménez, *J. Catal.*, 2019, **369**, 415–426.
19 X.-M. Liu, G. Q. Lu, Z.-F. Yan and J. Beltramini, *Ind. Eng. Chem. Res.*, 2003, **42**, 6518–6530.
20 R. Gaikwad, A. Bansode and A. Urakawa, *J. Catal.*, 2016, **343**, 127–132.
21 A. Bansode and A. Urakawa, *J. Catal.*, 2014, **309**, 66–70.
22 S. K. Wilkinson, L. G. A. Van De Water, B. Miller, M. J. H. Simmons, E. H. Stitt and M. J. Watson, *J. Catal.*, 2016, **337**, 208–220.
23 Y. Choi and H. G. Stenger, *Appl. Catal., B*, 2002, **38**, 259–269.
24 N. Boukis, V. Diem, W. Habicht and E. Dinjus, *Ind. Eng. Chem. Res.*, 2003, **42**, 728–735.
25 J. T. Sun, I. S. Metcalfe and M. Sahibzada, *Ind. Eng. Chem. Res.*, 1999, **38**, 3868–3872.
26 J. G. van Bennekom, R. H. Venderbosch, J. G. M. Winkelman, E. Wilbers, D. Assink, K. P. J. Lemmens and H. J. Heeres, *Chem. Eng. Sci.*, 2013, **87**, 204–208.

 